Journal of
Materials Chemistry A

Accepted Manuscript

This article can be cited before page numbers have been issued, to do this please use: Z. Lin, G. Liu, Y. Zheng, Y. Lin and Z. Huang, *J. Mater. Chem. A*, 2018, DOI: 10.1039/C8TA08225A.

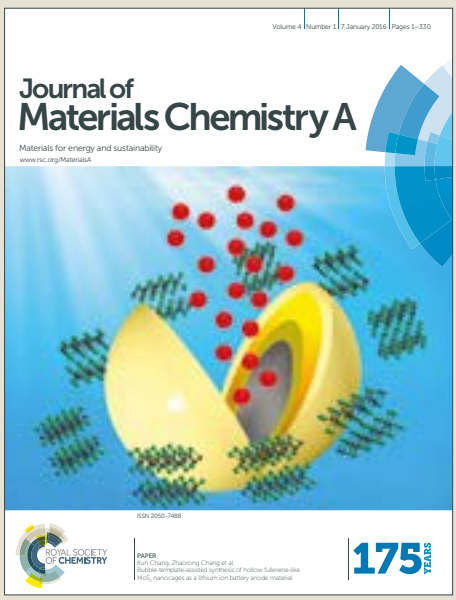

ROYAL SOCIETY OF CHEMISTRY

rsc.li/materials-a

View Article Online
DOI: 10.1039/C8TA08225A

Journal Name

ARTICLE

Three-dimensional hierarchical mesoporous flower-like TiO_2@graphdiyne with superior electrochemical performances for lithium-ion batteries

Received 00th January 20xx,
Accepted 00th January 20xx

DOI: 10.1039/x0xx00000x

www.rsc.org/

Zhiya Lin[a,b,c], Guozhen Liu[a,b], Yongping Zheng[a,b], Yingbin Lin*[a,b,c] and Zhigao Huang[a,b,c]

Three-dimensional hierarchical flower-like TiO_2@graphdiyne are prepared via a solvothermal process, and the structual properties and electrochemical performances are systematically investigated. The obtained results show that TiO_2@graphdiyne delivers high reversible capacities of 432.4 $mAhg^{-1}$ after 300 cycles at a current density of 1 Ag^{-1}, about 3 times that (139.7 $mAhg^{-1}$) of the pristine TiO_2. The high reversible capacities, excellent rate capability and cycle stability of TiO_2@graphdiyne might be attributed to the hierarchical mesopority of graphdiyne with butadiyne linkages, which could not only provide interconnect innumerable active sites for lithium storage but also faciliate fast Li-ion diffusion. The built-in electric field deriving from the difference in work function between TiO_2 and graphdiyne, could facilitate electron-transfer and Li-ion migration across heterojunction interfaces. Moreover, electron percolation and local built-in electric field induced by oxygen vacancies in TiO_2 matrix, could also enhance the kinetic of Li-ion insertion/deinsertion.

1. Introduction

Over the past decades, rechargeable lithium-ion batteries (LIBs) with high energy density and long cycling life, have received increasing attention in energy storage systems such as portable electronic devices, electric vehicles and large-scale energy storage.[1-3] Transition metal oxides are considered as promising candidates as the anode materials of high energy-density LIBs because of their various morphological characteristics and multiple chemical valence states.[4, 5] Among the numerous candidates investigated, titanium dioxide (TiO_2) has attracted extensive interest due to its good reversible capacity, structural stability and environmental friendliness.[6,7] Unfortunately, the intrinsically low lithium-ion mobility and poor electrical conductivity are still challenges that limit their high-rate performance in practical applications. To address the issues mentioned above, several strategies have been proposed including reducing the Li-ion diffusion length, designing hierarchically structure, doping with isovalent ions and coupling with conducting substances.[8-12] Among various methods mentioned above, carbon-coupling has been regarded as an effective way to improve the electrochemical performances, which not only establishes a stable interface to minimize side reactions with electrolyte but also enhances the electronic conductivity of TiO_2. [13-17] For example, Cai *et al.* [15] reported a walnut-like porous TiO_2@C core/shell exhibiting a high reversible capacity and an excellent rate capability of 126.4 $mAhg^{-1}$ at 20 C. Mo *et al.*[16] prepared TiO_2 quantum-dot/graphene nanosheet composites delivering superlative cyclic capacity retention at different current rates excellent high-rate performance at a current rate as high as 50 C. [17] It is well established that high capacity of carbon-coating TiO_2 composite with high rate performances is always highly desirable for LIBs application. Interestingly, graphdiyne, 2D carbon allotrope containing both sp and sp^2 hybridized carbon, seems to be a promising candidate because of typical triangular pores in framework, high specific surface area and high electrical conductivity as well.[18,19] Simultaneously, graphyne is also found to be a good intercalation electrode with high storage capacity (1480 $mAhg^{-1}$) and high lithium mobility, holding lithium ion in in-plane nanopores and relieving the volume change.[20,21] Moreover, the accessibility of the in-plane nanopores facilitates fast Li-ion diffusion along 3D channels, resulting in excellent rate performances and cycle stability at high lithiation/delithiation rates. [22,23]

[a] College of Physics and Energy, Fujian Normal University, Fujian Provincial Key Laboratory of Quantum Manipulation and New Energy Materials, Fuzhou , 350117, China.
[b] Fujian Provincial Engineering Technology Research Center of Solar Energy Conversion and Energy Storage, Fuzhou,350117, China.
[c] Fujian Provincial Collaborative Innovation Center for Optoelectronic Semiconductors and Efficient Devices, Xiamen, 361005, China.
† E-mail: yblin@fjnu.edu.cn; Fax: +86 591-2286-8132; Tel: +86 591-2286-8132

View Article Online
DOI: 10.1039/C8TA08225A

Herein, a 3D hierarchical mesoporous flower-like TiO_2 wrapped with graphdiyne synthesized by a simple solvothermal method. The obtained TiO_2@graphdiyne exhibits high reversible capacities, excellent rate capability and cycle stability because of additional storage sites for lithium ions, enhanced defect electrical conductivity, interfacial electric field due to different work function.

2. Experimental section

2.1 Synthesis of graphdiyne powders

The graphdiyne powers were prepared according to Prof. Li excellent work. [22-24] Typically, copper foils were dipped in 0.1 M hydrochloric acid overnight and subsequently washed with distilled water, ethanol and acetone several times. The resulting copper foils were added to the mixed solution of acetone, pyridine and tetramethylethylenediamine, with a volume ratio of 10:1:1 in a three-neck flask. Then 200 mg of hexakis[(trimethylsilyl)ethynyl]benzene dissolved in 50 mL of acetone was added immediately into above mixed solution. The mixture was kept stirring at 80 °C in an argon atmosphere with the help of a cryostat. After the reaction for 30 h, a black film appeared on copper foil, and precursor powders were left after evaporation of pyridine. The obtained precursor powders were further washed with acetone, hot dimethylformamide, and ethanol to remove other impurities. To get rid off metallic ions and other inorganic salt, the powder was then washed several additional times with 2 M HCl, 4 M NaOH, deionization water and ethanol. Finally, the obtained powers were annealed at 400 ℃in Ar atmosphere for 1 h.

2.2. Synthesis of TiO_2 and TiO_2@graphdiyne powders

Flower-like TiO_2 powders were synthesized by a solvothermal process using tetraisopropyl titanate (TBOT) as precursor. In a typical process, 5 mL glycerol was dissolved in 30 mL absolute ethyl alcohol, followed by added dropwise with 0.9 mL TBOT under magnetic stirring. After stirring for 10 minutes, the resulting suspension was transferred into a Teflon-lined stainless steel autoclave, sealed and maintained at 180 °C for 24 h. The precipitates were separated by centrifugation, washed with deionized water and alcohol, and then dried overnight. Eventually, the as-prepared precursor was calcined in Ar atmosphere at 450 °C for 3h to achieve well-crystallized TiO_2 powders. The synthesis of TiO_2@graphdiyne was similar to that of TiO_2, with graphdiyne disperse in glycerol and absolute ethyl alcohol mixed solution.

2.3 Materials characterization

The crystalline structures of the as-prepared composites are characterized by X-ray diffraction (XRD) using a Rigaku MiniFlex diffractometer with a Cu Kα radiation source (λ =0.15406 nm). The carbon structure of TiO_2@graphdiyne is examined by Raman spectroscopy using a LabRAM HR HORIBA JobinYvon spectrometer with the 532 nm excitation. Scanning electron microscope (SEM) images are obtained on a Hitachi SU8010 field-emission scanning electron microscope equipped with an energy-dispersive spectroscopy. Microstructure of TiO_2@graphdiyne is further identified using high-resolution transmission electron microscopy (Tecnai G2 F20 S-TWIN). The chemical composition and valence states of TiO_2@graphdiyne are characterized with on an X-ray photoelectron spectroscopy (ESCALAB 250Xi, Thermo Scientific). The graphdiyne content in composite is determined by thermo-gravimetric analysis (TGA, Netzsch STA449F3) from 30 to 600 °C at a heating rate of 3 °Cmin^{-1} under an air atmosphere. The surface potentials of TiO_2 and TiO_2@graphdiyne are measured by Kelvin probe atomic force microscopy (Bruker dimension ICON, Germany).

2.4 Electrochemical measurements

Working electrode was prepared by a slurry coating procedure. The slurry consisted of 70 wt% active materials (TiO_2 or TiO_2@graphdiyne), 20 wt% conductive Super P, 10 wt% poly(vinylidene fluoride) binder and N-methyl-2-pyrrolidone (NMP) solvent, and was uniformly coated onto a copper foil which was rinsed with water and alcohol. After vacuum drying at 120 °C for 12 h, electrode discs with a diameter of 12.5 mm were punched out and weighed. The loading density of the active materials was ~ 1.5 mg•cm^{-2}. For electrochemical measurements, the R2025 coin cells were assembled in an argon-filled glove box (H_2O and O_2 < 1 ppm) with metallic lithium foil as anode and counter electrode, Celgard 2300 microporous polyethylene membrane as separator and 1M $LiPF_6$ in a mixture of ethyl carbonate (EC) and dimethyl carbonate (DMC) (1:1 in vol. ratio) as electrolyte. The galvanstatic charge/discharge measurements of the cells were carried out by a multichannel battery testing system (LAND CT2001A, China) with a potential window ranging from 0.01 to 3.0 V at various current densities. Cyclic voltammograms (CV) measurements were performed by Arbin BT-2000 instruments, and electrochemical impedance spectra (EIS) were obtained using a Zahner Zennium electrochemical workstation in the frequency range of 10 mHz to 100 KHz with AC signal amplitude of 5 mV.

3. Results and discussion

3.1 Morphological and physical characterization

The typical surface morphologies of TiO_2 and TiO_2@graphdiyne powders are characterized with scanning electron microscopy, shown in Figs. 1 (a, b). Both samples demonstrate hierarchical flower-like architectures consisting of self-assembled radial nanorods with high surface area and TiO_2 nanorod consists of tiny well-crystalline particles,

View Article Online
DOI: 10.1039/C8TA08225A

presented in (Fig.1(c)). Fig.1(b) reveals that TiO_2 architectures are uniformly wrapped by gauze-like graphdiyne nanosheets, which could not only enhance the structural stability of TiO_2 hierarchical architectures but also facilitate charge transfer because of a highly conductive graphdiyne-network in composite. TEM image shown in Fig. 1(d) further confirms the uniformity distribution of the graphdiyne in TiO_2@graphdiyne. In addition, the distance of the visible lattice fringes is ca. 0.35 nm, corresponding to the (101) lattice plane of anatase TiO_2.[25] The composition and element distribution in TiO_2@graphdiyne are examined by energy dispersive spectroscopy. Fig. 2 reveals the existence and homogeneous distribution of Ti, O and C elements throughout the selected zone of TiO_2@graphdiyne powder.

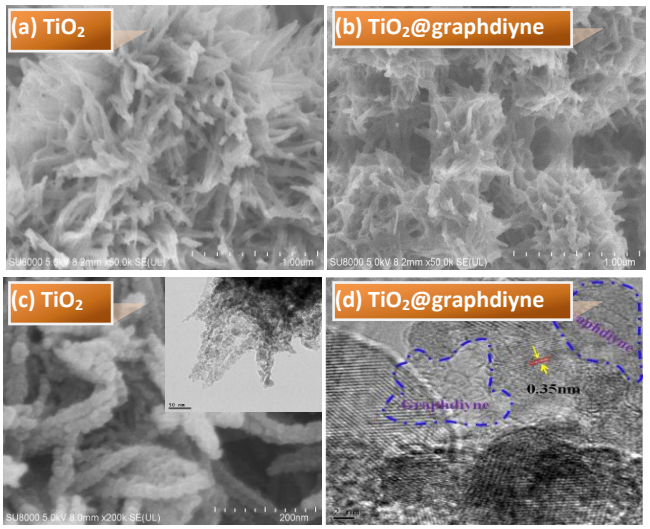

Fig.1 (a, b) SEM morphologies and (c, d) TEM images of TiO_2 and TiO_2@graphdiyne powders

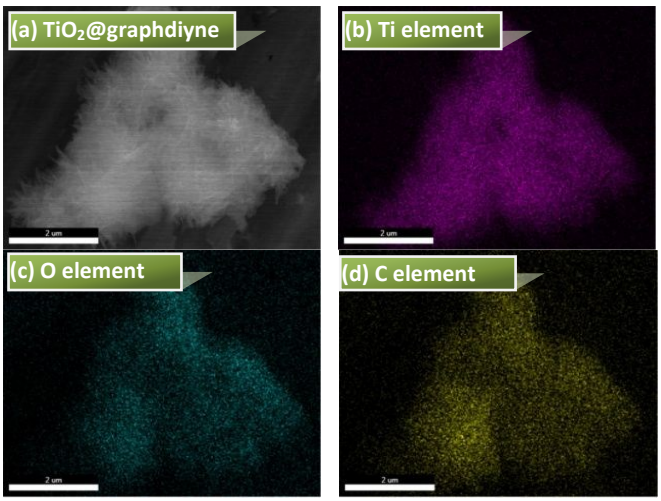

Fig.2 Element maps of TiO_2@graphdiyne particles.

Fig. 3(a) shows the typical Raman spectra of the as-prepared graphdiyne. The peaks appeared around 1380 and 1578 cm^{-1} are unambiguously assigned to the breathing mode of k-point phonons of A_{1g} symmetry (D band) and first-order scattering of the E_{2g} mode for in-phase stretching vibration of the sp^2 carbon lattice (G band).[19] Two tiny peaks around 1938 and 2186 cm^{-1} are ascribed to the vibration of conjugated diyne links(-C≡C-C≡C-).[24] The relative intensity ratio of D band to G band indicates the low defects and high graphitization degree of graphdiyne, which facilitates electron transfer in composites. [18] Fig.3(b) shows the XRD patterns of TiO_2 and TiO_2@graphdiyne. All the diffraction peaks of the as-prepared composites can be well indexed to anatase TiO_2 (JCPDS 21-1272).[32] To quantify the amount of graphdiyne in the TiO_2@graphdiyne composites, thermogravimetric analysis is carried out, Fig.3(c) reveals that the amount of graphdiyne in TiO_2@graphdiyne composite is about 24 wt%.

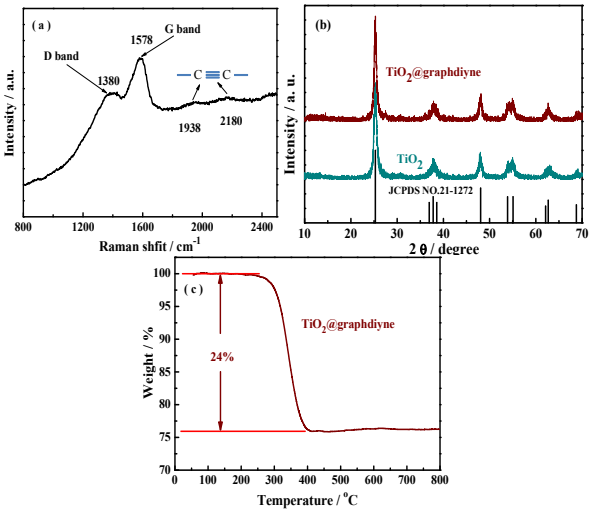

Fig.3 (a) Raman spectrum of the as-prepared graphdiyne powders; (b) XRD patterns of TiO_2 and TiO_2@graphdiyne powders; (b) TG curve of the TiO_2@graphdiyne.

View Article Online
DOI: 10.1039/C8TA08225A

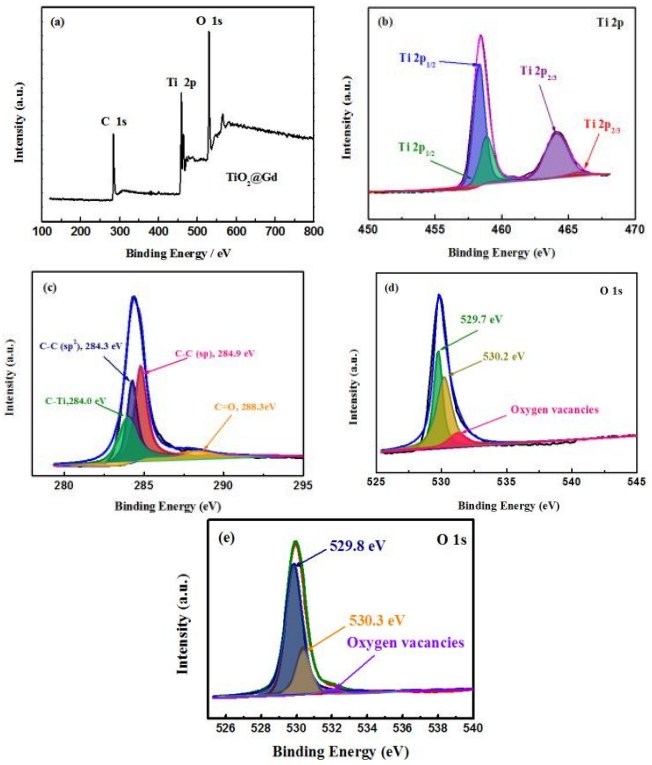

Fig.4 XPS spectra of (a) survey spectra, (b) Ti2p, (c) C 1s and (d) O1s of TiO_2@graphdiyne samples; (e) O1s of TiO_2 for comparison.

The chemical composition and valence state of TiO_2@graphdiyne are characterized with X-ray photoelectron spectroscopy. As shown in Fig.4(a), the survey XPS spectra reveals that the dominant elements are Ti, O and C in TiO_2@graphdiyne composite. The characteristic bands located around 458.4 and 464.1 eV (Fig.4(b)) are attributed to Ti $2p_{3/2}$ and Ti $2p_{1/2}$ spin-orbit doublets, indicating the predominant state of Ti element is Ti^{4+} in composite.[26] In addition, two additional peaks around 458.9 and 465.7eV are related to the Ti $2p_{1/2}$ and Ti $2p_{3/2}$ spin-orbital splitting photoelectrons from C-Ti bonds and the low valence state of Ti^{3+},[27, 28] further confirming the formation of chemical bond between TiO_2 and graphdiyne. The C 1s peak shown in Fig .4(c) can be well fitted with four main sub-peaks at 284.0, 284.3, 284.9 and 288.3 eV, assigning to orbitals in C-Ti, C-C (sp2), C-C (sp) and C = O bonds respectively.[24,29] The appearance of C-Ti and C=O bonds indicates the strong adhesion between TiO_2 and graphdiyne, which is thereby beneficial for the charge transfer in the composites and mitigate aggregation of TiO_2 nanoparticles during the Li-ion insertion/deinsertion process. Fig. 4(d) show the fitting curves of the O 1s peak of the composite, and each of them can mainly be decomposed into two peaks located at ~529.7 and ~530.2 eV, which are ascribed to lattice oxygen and near-surface oxygen like molecular water adsorbed on the surface, respectively.[30] Moreover, a new weakly peak located at 531.5 eV is observed in the TiO_2@graphdiyne sample, which can be assigned to oxygen vacancies.[30,31] In comparison, the peak corresponding to oxygen vacancies is hardly observed in O 1s peak of TiO_2 sample, shown in Fig.4(e).

3.2 Electrochemical measurements

The rate performances of TiO_2 and TiO_2@graphdiyne electrodes between 0.01~3V at various current rates are investigated and is presented in Fig.5(a). Comparing to the pristine TiO_2, TiO_2@graphdiyne delivers higher capacities especially at higher current density. As the current density increases, TiO_2@graphdiyne electrodes have reversible discharge capacities of 493.8, 429.0, 399.7, 361.9 and 284.7 $mAhg^{-1}$ respectively, while the capacities of TiO_2 electrodes are only 306.7, 236.1, 214.9, 180.1 and 122.1 $mAhg^{-1}$. The enhanced rate capability of TiO_2@graphdiyne electrode could be attributed to the fact that the cross-linked high-conductive graphdiyne networks facilitate the charge transfer and consequently reduce the polarization of the electrode. On the other hand, the high capacities of TiO_2@graphdiyne also result from the unique structure of graphdiyne with numerous triangular pores which endow graphdiyne with lots of Li storage sites and facilitate insertion/extraction and diffusion of Li ions both out-of-plane and in-plane.[33] Fig. 5(b) shows cyclic voltammetry of TiO_2 and TiO_2@graphdiyne electrodes between 0.01 and 3.0 V at a scanning rate of 0.1 mVs^{-1}. Both electrodes demonstrate cathodic insertion of lithium at ~1.65 V and anodic extraction of lithium at ~2.1 V versus Li/Li^+ , respectively. These anodic/cathodic peaks correspond to the Li-ion extraction/insertion from/to the anatase lattice.[34] In comparison, TiO_2@graphdiyne has a smaller voltage difference (0.27 V) between the cathodic and anodic peaks than that (0.55 V) of the pristine one, reflecting the lower polarization of the electrode by hybriding with graphdiyne.

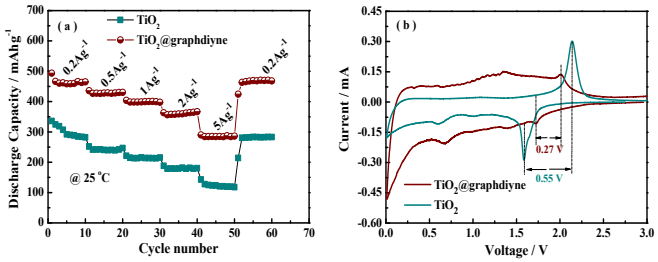

Fig.5 (a) The rate capability of TiO_2 and TiO_2@graphdiyne electrodes; (b) CV curves of TiO_2 and TiO_2@graphdiyne electrodes at a scanning rate of 0.1 mVs^{-1}.

The influence of graphdiyne-hybriding on the Li-ion kinetic behavior is further investigated by Kelvin probe atomic force microscopy in terms of work function, reflecting the minimum

View Article Online
DOI: 10.1039/C8TA08225A

energy required for the loss of an electron from the inside of a bulk material to the vacuum. Fig. 6(a,b) presents the surface potential images over a scan area of 200nm×200nm of TiO_2 and TiO_2@graphdiyne composites. Fig. 6(c) shows the surface potential image of Au foil serving as calibration sample whose work function (Φ_{Au}) is 5.31 eV. Based on our previously work reported,[35] the work functions of TiO_2 and TiO_2@graphdiyne are calculated and the corresponding results are presented in Fig. 6(d). It is clear that TiO_2@graphdiyne has a smaller work function (5.08 eV) than that (5.70 eV) of the TiO_2. The measured work function of TiO_2 is equal to the reported value (5.7 eV).[36] Smaller work function requires less energy for electrons to escape from the composite. Therefore, graphdiyne-hybriding is expected to facilitate electron transfer in electrode, which is consist with the analysis of CV measurements.

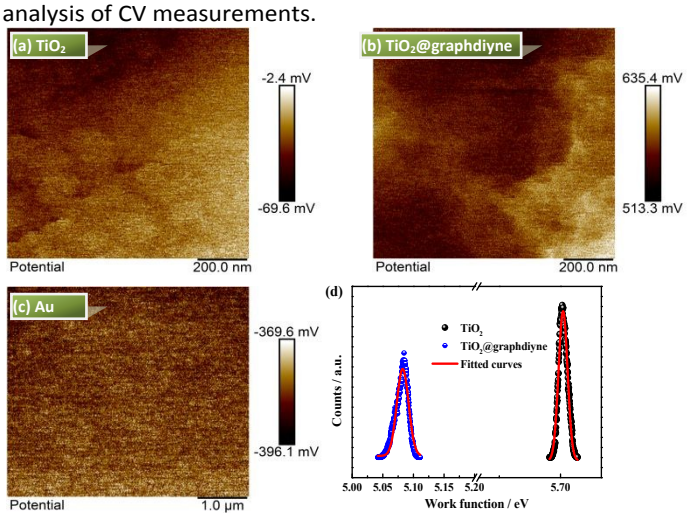

Fig.6 The surface potential maps of (a) TiO_2 and (b) TiO_2@graphdiyne electrodes; (c) the surface potential map of Au as reference sample; (d) Work functions of TiO_2 and TiO_2@graphdiyne electrodes.

Fig. 7(a) presents cycling performance of TiO_2 and TiO_2@graphdiyne at 1 Ag^{-1} in the voltage range of 0.01~3.0 V. TiO_2@graphdiyne has a higher discharge capacity and exhibits superior cycling stability. TiO_2@graphdiyne electrode deliver a reversible capacity of 432.4 $mAhg^{-1}$ after 300 cycles while TiO_2 electrode is merely 139.7 $mAhg^{-1}$. The rising capacity of TiO_2@graphdiyne during the initial 100 cycles might be related with two phenomena: a) a gradual activation of graphdiyne during conversion process,[19] and b) the porous structure of graphdiyne providing additional storage sites for Li atoms.[29] The comparison summarized in Table 1 reveals the superior electrochemical performances of TiO_2@graphdiyne, indicating its potential application in high-energy lithium-ion batteries. To further insight into the cycling stability of TiO_2@graphdiyne, the morphologies of TiO_2 and TiO_2@graphdiyne electrodes at 0.01 V after 300 cycles test are studied, shown in Fig. 7(b,c). It is clear that TiO_2 powders have serious structure-deterioration and losses its flower-like morphologies, increasing interfacial resistance among particles and reducing the contact areas between active materials and the electrolyte. In contrast, TiO_2@graphdiyne powders can remain in the flower-like structure well, indicating that graphdiyne-hybriding would stabilize structure of the active materials and consequently provide more lithium-ion insertion/extraction active sites.

Table The comparison of electrochemical performances between our work and other's reports

Materials	Voltage range / V	Current density/rate	Capacity / $mAhg^{-1}$	Ref.
TiO_2@CNTs	0.01~3	0.027 Ag^{-1}	220 after 60 cycles	[38]
TiO_2@MoO_3	0.005~3	0.5 Ag^{-1}	365.9 after 100 cycles	[39]
TiO_2@C	0.01~3	1 Ag^{-1}	270.1 after 500 cycles	[37]
TiO_2@PPO	0.01~3	2.4 C	225 after 200 cycles	[44]
TiO_2@Fe_2O_3	0.01~3	0.2 Ag^{-1}	450 after 150 cycles	[14]
$Ti_{0.85}Sn_{0.15}O_2$	0.05~3	0.382 Ag^{-1}	230 after 500 cycles	[45]
TiO_2@Graphdiyne	0.01~3	1 Ag^{-1}	432.4 after 300 cycles	this work

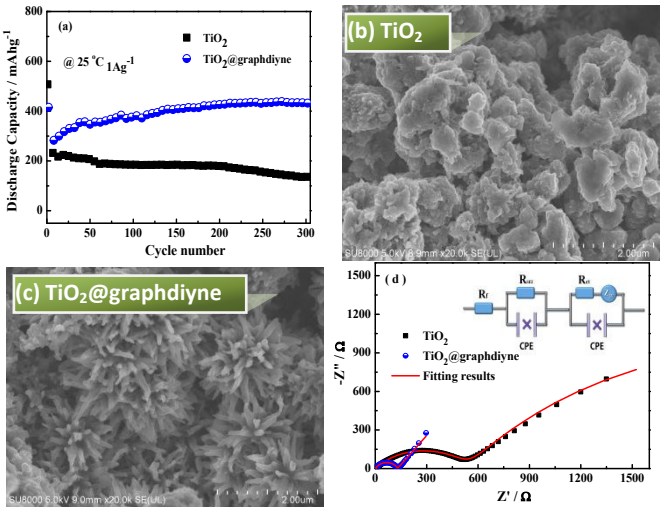

Fig.7 (a) Cycling performance of TiO_2 and TiO_2@graphdiyne at 1Ag^{-1}; (b,c) Surface morphologies of TiO_2 and TiO_2@graphdiyne electrodes after 300 galvanostatic charge/discharge cycles; (d) EIS profiles of TiO_2 and TiO_2@graphdiyne at discharged state; Inset: the equivalent circuit for EIS fitting.

Fig. 7(d) shows the Nyquist plots of the TiO_2 and TiO_2@graphdiyne electrodes in the frequency range from 100 KHz to 10 mHz. Both EIS curves are composed of a compressed semicircle at the medium frequency region and a straight sloping line in the low frequency region. Based on the equivalent circuit in the inset of Fig. 7(d),[37] the charge-transfer resistance (R_{ct}) for TiO_2 and TiO_2@graphdiyne are calculated as 536.6 and 126.4 Ω, respectively, indicating the enhanced reaction kinetics induced by high-conductivity graphdiyne-hybriding and stable structure. In addition, chemical bond (Ti-C bond) between TiO_2 and

View Article Online
DOI: 10.1039/C8TA08225A

graphdiyne could also facilitate electron-transfer across across heterojunction interfaces, and efficiently suppress SEI-film growth between them. On the other hand, the adhesion force between TiO_2 and graphdiyne is expected to avoiding the agglomeration of the TiO_2 nanoparticles during the charge/discharge process, and suppress an increase of interfacial resistance among particles.

To further investigate the effect of graphdiyne-hybriding on the Li^+ diffusion kinetics of TiO_2, the impedance spectra of TiO_2 and TiO_2@graphdiyne are continuously measured during the lithium-ion insertion/extraction process, shown in Fig. 8(a-d). The corresponding lithium-ion diffusion coefficient (D_{Li^+}) could be calculated based on the linear relationship between the real axis (Z′) and the reciprocal square root(ω-1/2) in the low frequency region.[42] Fig. 8(e,f) presents lithium-ion diffusion kinetics of TiO_2 and TiO_2@graphdiyne during the lithium-ion insertion/extraction process. Both electrodes exhibit similar Li-ion diffusion behavior and display two peaks at ~1.7 and ~2.0V, corresponding to the redox reactions of the Ti^{3+}/Ti^{4+} couple in TiO_2. It is obvious that TiO_2@graphdiyne electrode has better Li-ion diffusion kinetics and smaller difference between insertion and de-insertion peak, suggesting that graphene-hybriding would readily facilitate Li-ion diffusion and reduce electrode polarization during the lithium-ion insertion/extraction process. On the other hand, it is found that the reversibility of lithium electrochemical intercalation/extraction for TiO_2@graphdiyne electrode is better than that of the pristine one in a potential voltage from 1.0 to 0.01V.

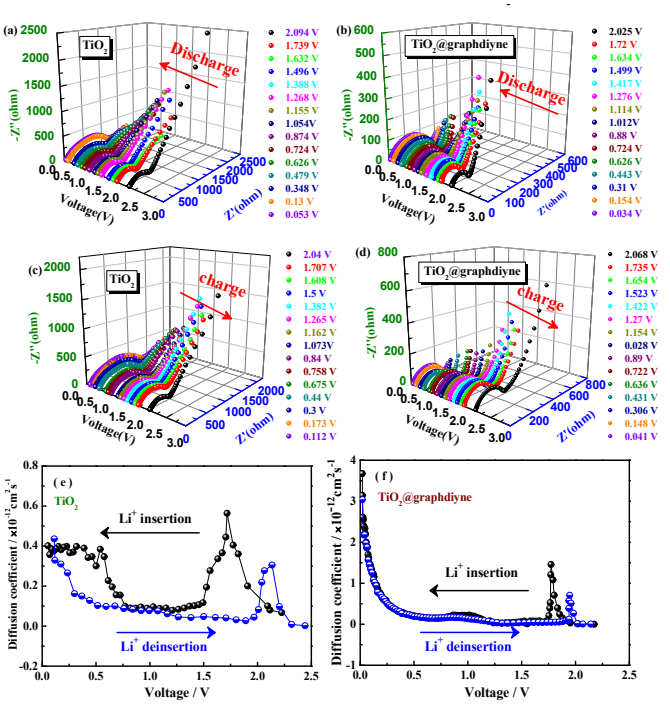

Fig.8 (a-d) The impedance spectra of TiO_2 and TiO_2@graphdiyne electrodes under different charge/discharge states; (e, f) Lithium ion diffusion coefficients at different charge/discharge states for TiO_2 and TiO_2@graphdiyne electrodes.

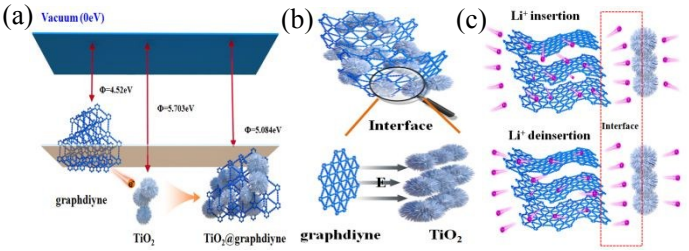

Fig.9 (a) The energy-level model for explaining the enhanced electron transfer in TiO_2@graphdiyne; (b, c) An interfacial built-in electric field (E) between TiO_2 and graphdiyne, which facilitates charge transfer across the interface.

Potential mechanisms for electrochemical performance enhancement of TiO_2@graphdiyne could be well explained in terms of built-in electric field at the heterostructure interface and point defects such as oxygen-vacancy as well. Due to the difference in work functions between TiO_2(~5.70 eV) and graphdiyne(~4.52 eV),[36,43] electrons transfer occurs from graphdiyne to TiO_2 until the two Fermi levels are aligne. [44] Therefore, a corresponding electric field (E) is built up at the heterostructure interface, shown in Fig.9(b). Such built-in electric field could facilitate Li-ion diffusion from graphdiyne to TiO_2, and electron transfer from TiO_2 to graphdiyne across heterojunction interfaces, shown in Fig.9(c).

The oxygen-vacancies in TiO_2 matrix seem to be a non-negligible factor for improving Li-ion kinetics in terms of percolation charge transfer and the local built-in electric field. Due to the imbalance charge distribution induced by oxygen vacancies, a positive-charged area in the oxygen-vacancy center and an equivalent negative-charged electron area surrounding the oxygen vacancies are correspondingly formed, [31] shown in Fig.10 (a). The radius of the electron orbital is of the order εa_0, where ε is the dielectric constant of TiO_2 and a_0 is the Bohr radius.[45] As the oxygen vacancy concentration is beyond the percolation limit, the negative-charged electron areas start to overlap to form a continuous chain throughout TiO_2 matrix (shown in Fig.10 (b)) and consequently enhance de-localized electron transfer in materials, which is similar to the bound magnetic polarons theory of oxygen-vacancy magnetic semiconductor.[46] It is worth noticing that the local built-in electric field origining from the lopsided charge distribution around the oxygen vacancy area should be responsible for the enhanced electrochemical performances in TiO_2@graphdiyne. During the discharging processes, the local built-in electric field

View Article Online
DOI: 10.1039/C8TA08225A

pointing from the defect-free region to the negative-charged overlapped-chain would accelerate Li-ion migration and induce them to gather around the oxygen-vacancy region because of the coulombic forces, [31] shown in Fig.10(c). After deep discharging, the negatively charged region becomes electrically neutral. During the charging processes, the secondary electric field, pointing from positive-charged oxygen-vacancy center to electroneutral lithiation layer including graphdiyne, would also facilitate Li-ion extraction in TiO_2 matrix and across heterojunction interfaces, shown in Fig.10(d). As a result, the electrochemical performances are enhanced.

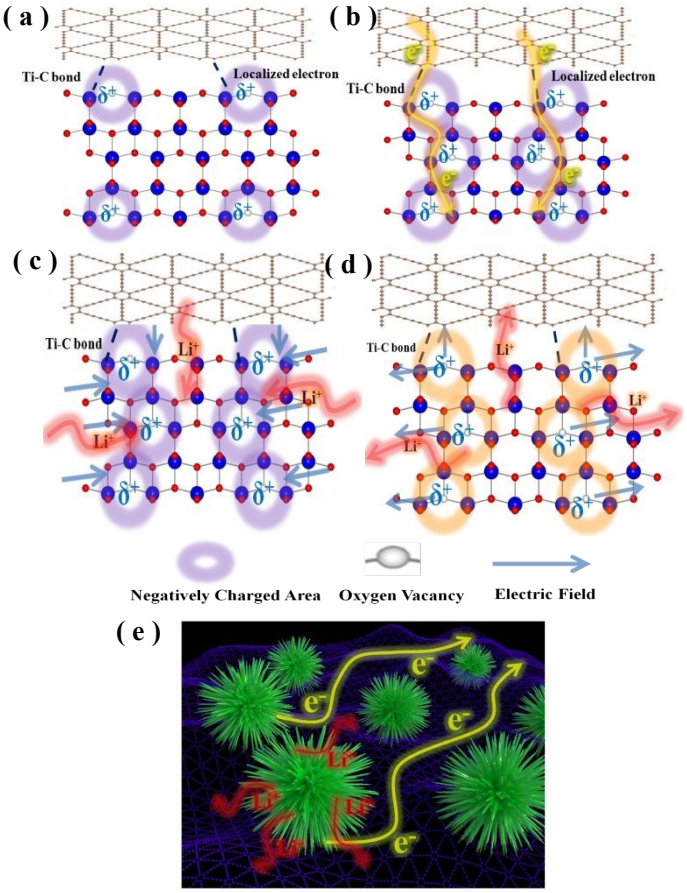

Fig.10 (a) a positive-charged area in the oxygen vacancy center and an equivalent negative-charged electron area surrounding the oxygen vacancies; (b) The de-localized electron transfer throughout TiO_2 matrix under the help of oxygen vacancies; (c, d) Schematic illustration of potential mechanism behind the improved electrochemical performances due to the oxygen vacancy derived local built-in electric field; (e) Schematic illustration of the enhanced electrochemical performances in TiO_2@graphdiyne electrodes.

4. Conclusions

In summary, three-dimensional hierarchical flower-like TiO_2@graphdiyne composites have been successfully prepared by a solvothermal process followed by thermal annealing in Ar atmosphere. The as-prepared TiO_2@graphdiyne exhibits superior electrochemical performances in terms of high reversible capacities, excellent rate capability and better cycling stability. The enhanced performances of TiO_2@graphdiyne might be attributed to the hierarchical mesopority of graphdiyne with butadiyne linkages, electron percolation and built-in electric field induced by oxygen vacancies. This work may open a new avenue for the design and synthesis of graphdiyne-based composites for high-performance Li ion battery.

Conflicts of interest

There are no conflicts to declare.

Acknowledgements

This work was supported by the Key Project of Department of Science & Technology of Fujian Province (No.2014H0020) and Program for New Century Excellent Talents in University of Fujian Province (No.JA14069).

References

1. D. H. Xu, F. L. Yu, C. Liu, P. D. Han, B. C. Weng, J. Power Sources **2017**, 354, 85.
2. Y. Yang, S. T. Wang, S. Lin, Y. T. Li, W. Y. Zhang, Y. G. Chao, M. C. Luo, Y. Xing, K. Wang, C. Yang, P. Zhou, Y. L. Zhang, Z. L Tang and S. J. Guo, Small Methods **2018**, 1800119.
3. W. S. Weng, J. Lin, Y. C. Du, X. F. Ge, X. S. Zhou and J. C. Bao, J. Mater. Chem. A **2018**, 6, 10168.
4. X. Liu, Y. C. Du, L. Y. Hu, X. S. Zhou, Y. F. Li, Z. H. Dai and J. C. Bao, J. Phys. Chem. C **2015**, 119, 5848.
5. X. S. Zhou, Y. X. Yin, A. M. Cao, L. J. Wan and Y. G. Guo, ACS Appl. Mater. Interfaces **2012**, 4, 2824.
6. M. Dahl , Y. D. Liu , Y. D. Yin , *Chem. Rev.* **2014**, 114, 9853.
7. L. J. Zhao, S. T. Wang, F. Pan, Z. L. Tang, Z. T. Zhang, S. W. Zhong and J. Y. Zhang, J. Mater. Chem. A **2018**, 5, 11688.
8. D. Pan, H. Huang, X. Wang, L. Wang, H. Liao, Z. Li, M. Wu, *J. Mater. Chem. A* **2014**, 2, 11454.
9. H. Han, T.Song, J. Y. Bae, L. F. Nazar, H. Kim, U. Paik, *Energy Environ. Sci.* **2011**, 4, 4532.
10. M. Lübke, I. Johnson, N. M. Makwana, D. Brett, P. Shearing, Z. L. Liu , J. A. Darr, *J. Power Sources* **2015**, 294, 94.
11. F. F. Cao, S. Xin, Y. G. Guo, L. J. Wan, *Phys. Chem. Chem. Phys.* **2011**, 13, 2014.
12. J. X. Duan, H. Y. Hou, X. X. Liu, Q. S. Liao, S. Liu, R. J. Meng, Z. L. Hao, Y. Yao, *J. APPL. POLYM. SCI.* **2016** 43685.
13. J.W. Zhang, X.X. Yan, J.W. Zhang, W. Cai, Z.S. Wu, Z.J. Zhang, *J. Power Sources* **2012**, 198, 223.
14. R. Qing, L. Liu, H. Kim, W. M. Sigmund, *Electrochim. Acta* **2015**, 18, 295.
15. Y. Cai, H. E. Wang, X. Zhao, F. Huang, C. Wang, Z. Deng, Y. Li, G. Z. Cao, B. L. Su, *ACS Appl. Mater. Interfaces* **2017**, 9, 10652.

View Article Online
DOI: 10.1039/C8TA08225A

16. R. W. Mo, Z. Lei, K. N. Sun, D. Rooney, *Adv. Mater.* **2014**, 26, 2084.
17. S. J. Ding, J. S. Chen, D. Y. Luan, F. Y. Chiang Boey, S. Madhavibc and X. W.(David) Lou, *Chem. Commun.* **2011**, 47, 5780.
18. C. S. Huang, S. G. Zhang, H. B. Liu, Y. J. Li, G. G. Cui, Y. L. Li, *Nano Energy* **2015,** 11, 481.
19. S. G. Zhang, H. B. Liu, C. S. Huang, G. G. Cui and Y. L. Li, *Chem. Commun.* **2015**, 51, 1834.
20. H. Shang, Z. C. Zuo, L. Yu, F. Wang, F. He and Y. L. Li, Adv. Mater. **2018**, 30, 1801459.
21. H. P. Du, H. Y., C. S. Huang, J. J. He, H. B. Liu, Y. L. Li, *Nano Energy* **2016**, 22, 615.
22. H. Shang, Z. C. Zuo, L. Li, F. Wang, H. B. Liu, Y. J. Li and Y. L. Li, *Angew. Chem.* **2017**, 129, 1.
23. Z. C. Zuo, H. S., Y. H. Chen, J. F. Li, H. B. Liu, Y. J. Li and Y. L. Li, *Chem. Commun.* **2017**, 53, 8074.
24. J. J. He, N. Wang, Z. L. Cui, H. P. Du, L. Fu, C.S. Huang, Z. Yang, X. Y. Shen, Y. P. Yi, Zeyi Tu & Y. L. Li, *Nat. Commun.* **2017**, 8, 1172.
25. G. Kim, C. S. Jo, W. Kim, J. Y. Chun, S. H Yoon, J. W Lee and W. Y Choi, *Energy Environ. Sci.* **2013**, 6, 2932.
26. Y. M. Li, J. R. Shen, J. J. Li, S. M. Liu, D. L. Yu, R. C. Xu, W. F. Fu and X. J. Lv, *J. Mater. Chem. A* **2017**, 5,7055.
27. X. Y. Zhang, H. P. Li, X. L. Cui, & Y. Lin, *J. Mater. Chem.* **2010,** 20, 2801.
28. O. Akhavan, & E. Ghaderi, *J. Phys. Chem. C* **2009**, 113, 20214.
29. K. Wang, N. Wang, J. J. He, Z. Yang, X. G. Shen, C. S. Huang, *Electrochim. Acta* **2017**, 253, 506.
30. T. F. Zhou, Y. Zheng, H. Gao, S. D. Min, S. Li, H. K. Liu and Z. P. Guo, *Adv. Sci.* **2015**, 2, 1500027.
31. C. X. Hou, Y. Hou, Y. Q.i Fan, Y. J. Zhai, Y. Wang, Z. Y. Sun, R. H. Fan, F. Dang and J. Wang, *J. Mater. Chem. A* **2018**, 6, 6967.
32. G. Lui, G. Li, X. L. Wang, G. P. Jiang, E. Lin, M. Fowler, A. P. Yu, Z. G. Chen, *Nano Energy* **2016,** 24,72.
33. J. Xu, J. Q. Li, Q. L. Yang, Y. Xiong, C. G. Chen, *Electrochim. Acta* **2017**, 251, 672.
34. C. Wang, L. X. Wu, H. Wang, W. H. Zuo, Y. Y. Li and J. P. Liu, *Adv. Funct. Mater.* **2015**, 25, 3524.
35. Z. Y. Lin, Y. M. Yang, J. M. Jin, L. Y. Wei, W. Chen, Y. B. Lin, Z. G. Huang, *Electrochim. Acta* **2017**, 254, 287.
36. F. Brivio, K. T. Butler, and A. Walsh, *Phys. Rev. B* **2014**, 89, 155204.
37. R. F. Wu, S. Y. Shen, G. F. Xia, F. J. Zhu, C. Lastoskie and J. L. Zhang, *ACS Appl. Mater. Interfaces* **2016**, 8, 19968.
38. P. Zhang, J. X. Qiu, Z. F. Zheng, G. Liu, M. Ling, W. Martens, H. H. Wang, H. J. Zhao, S. Q. Zhang, *Electrochim. Acta* **2013**, 104, 41.
39. Y. F. Li, Y. J. Hu, J. H. Shen, H. B. Jiang, G. Q. Min, S. J. Qiu, Z. T. Song, Z. Sun and C. Z. Li, *Nanoscale* **2015**, 7, 18603.
40. X. X. Lv, J. J. Deng, X. H. Sun, *Appl. Surf. Sci.* **2016**, 369, 314.
41. M. Lübke, I. Johnson, N. M. Makwana, D. Brett, P. Shearing, Z. L. Liu, J. A. Darr, *J. Power Sources* **2015**, 294, 94.
42. D. D. Wang, Z. Q. Shan, R. Na, W. L. Huang, J. H. Tian, *J. Power Sources* **2017**, 337, 11.
43. X. J. Dai, and D. H. Ge, *AIP Adv.* **2018**, 8, 015320.
44. B. Bhushan, Scanning probe microscopy in nanoscience and nanotechnology, Springer Heidelberg, Dordrecht London New York, **2017,** 46.
45. S. K.S. Patel, S. Kurian, N. S. Gajbhiye, *Mater. Res. Bull.* **2013**, 48, 655.
46. M. Y. Zhu, Z. H. Zhang, M. Zhong, M. Tariq, Y. Li, W. X. Li, H. M. Jin, K. Skotnicova, Y. B. Li, *Ceram. Inter.* **2017,** 4, 3166.

View Article Online
DOI: 10.1039/C8TA08225A

GRAPHICAL ABSTRACT

Three-dimensional hierarchical mesoporous flower-like TiO_2@graphdiyne with superior electrochemical performances for lithium-ion batteries

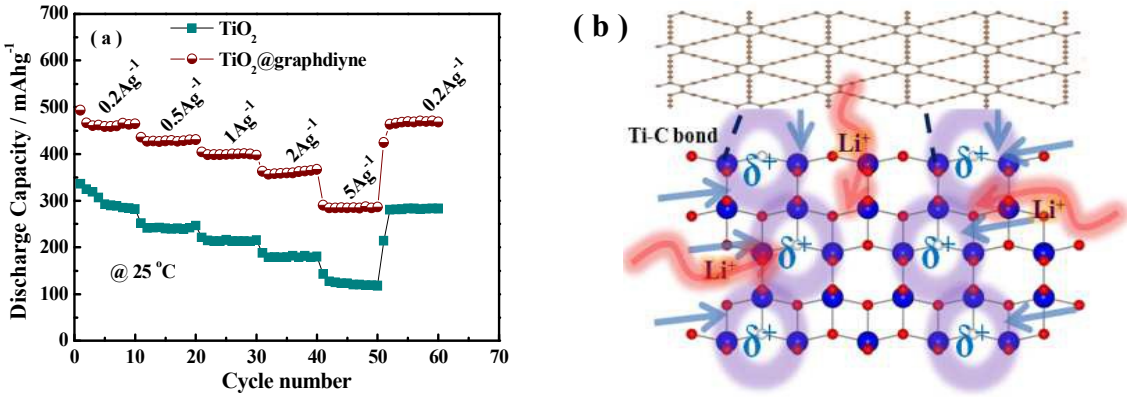

Three-dimensional hierarchical flower-like TiO_2@graphdiyne composites have been successfully prepared by a hydrothermal process followed by thermal annealing in Ar atmosphere. The as-prepared TiO_2@graphdiyne exhibits superior electrochemical performances in terms of high reversible capacities, excellent rate capability and beteer cycling stability. The enhanced performances of TiO_2@graphdiyne might be attributed to the hierarchical mesopority of graphdiyne with butadiyne linkages, electron percolation and built-in electric field induced by oxygen vacancies.